160-Gb/s Optically Time-Division Multiplexed Link with All-Optical Demultiplexing

Todd G. Ulmer, *Member, OSA*, Michael C. Gross, *Member, OSA*, Ketan M. Patel, Julaine T. Simmons, *Member, OSA*, Paul W. Juodawlkis, *Member, IEEE, Member, OSA*, Brian R. Washburn, William S. Astar, *Member, OSA*, Anthony J. SpringThorpe, Richard P. Kenan, *Senior Member, IEEE, Fellow, OSA*, Carl M. Verber, *Senior Member, IEEE, Fellow, OSA*, and Stephen E. Ralph, *Member, IEEE, Member, OSA*

***Abstract*—An ultrafast single-wavelength optically time-division multiplexed (OTDM) link is described. The link exploits a unique integrated, all-optical serial-to-parallel (S/P) converter based on second-harmonic generation that demultiplexes multiple high-speed optical channels with a single operation. The link is composed of five major components: 1) a high-repetition-rate picosecond-pulse source; 2) a planar waveguide multiplexer that incorporates electroabsorption modulators with integral spot-size converters (SSCs); 3) a dispersion-managed (DM) short-pulse fiber channel; 4) a quasi-phase-matched, resonant-cavity-enhanced AlGaAs waveguide designed for surface-emitted second-harmonic generation (SESHG); and 5) a 775-nm receiver optimized for return-to-zero (RZ) operation. We describe our recent advances with resonant cavity enhancement of the all-optical demultiplexer and the first bit error rate (BER) measurements for this demultiplexing scheme.**

***Index Terms*—All-optical demultiplexing, electroabsorption modulators, quasi-phase matching, return-to-zero (RZ) transmission, spot-size converter (SSC), time-division multiplexing (TDM).**

I. Introduction

ULTRAFAST single-wavelength transmission has attracted considerable attention as a means of increasing the capacity of future optical networks [1]–[3]. Indeed, advances in materials and devices expand the role of optical signal processing and thereby increase the choices available when selecting an appropriate mix of wavelength-division-multiplexing (WDM) and optical-time-division-multiplexing (OTDM) technologies. Ultrafast OTDM requires short-pulse transmission at rates up to 160 Gb/s (OC-3072) and greater. Recent single-wavelength demonstrations include a 100-Gb/s OTDM soliton system using a 20-Gb/s optical demultiplexing scheme with dispersion-managed (DM) fiber for transmission distances of 1000 km [4]. The role of these ultrahigh-data-rate OTDM techniques within a WDM system has been demonstrated in a 3-Tb/s experiment [5] where 19 wavelengths, each at 160 Gb/s, were transmitted over 40 km of dispersion-shifted fiber (DSF). Typically, these demonstrations use conventional modulator technology for temporal multiplexing and demultiplexing; however, all-optical methods based on nonlinear effects have also been demonstrated using fibers and semiconductors [6]. Here, we describe the components of an ultrafast optical link that exploits an integrated all-optical demultiplexer based on surface-emitted second-harmonic generation (SESHG) to enable the recovery of all OTDM channels with a single optical operation.

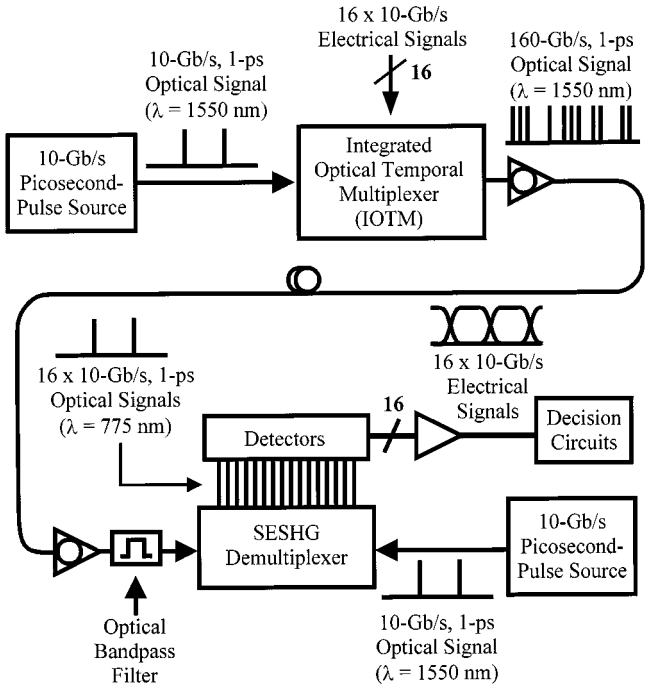

Fig. 1. Schematic of the 160-Gb/s OTDM point-to-point link. Sixteen 10-Gb/s electronic channels are optically multiplexed for transmission. An optical S/P converter based on SESHG demultiplexes the data back down to the electronic channel rate.

The primary elements of the 160-Gb/s single-wavelength OTDM link are shown in Fig. 1. An integrated-optical temporal multiplexer (IOTM) consisting of a hybridized semiconductor/silica waveguide circuit provides the basic building block of the multiplexer. This component, together with a picosecond-pulse source operating at the channel rate of 10-GHz, produces the system-rate 160-Gb/s aggregate data stream by multiplexing 16 channel-rate signals. These individual 10-Gb/s

Manuscript received April 27, 2000. This work was supported by BellSouth, Corning, Nortel Networks, and the Georgia Research Alliance through the Ultrafast Optical Communications Consortium.

T. G. Ulmer, M. C. Gross, K. M. Patel, B. R. Washburn, W. S. Astar, R. P. Kenan, C. M. Verber, and S. E. Ralph are with the Georgia Institute of Technology, Atlanta, GA 30332 USA (e-mail: stephen.ralph@ece.gatech.edu).

J. T. Simmons is with Lucent Technologies, Holmdel, NJ 07733 USA.

P. W. Juodawlkis is with the Massachusetts Institute of Technology (MIT) Lincoln Laboratory, Lexington, MA 02420 USA.

A. J. SpringThorpe is with Nortel Advanced Technology Laboratory, Ottawa, ON K2H 8E9, Canada.

Publisher Item Identifier S 0733-8724(00)10704-2.

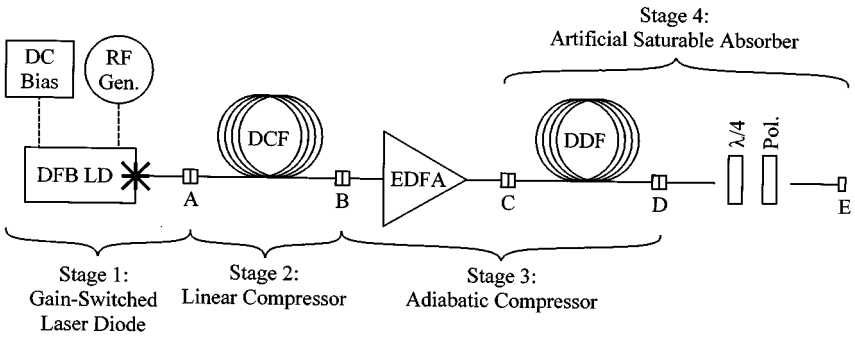

Fig. 2. Picosecond-pulse source. RF Gen.: RF generator. DFB LD: distributed-feedback laser diode. DCF: dispersion-compensating fiber. EDFA: erbium-doped fiber amplifier. DDF: dispersion- decreasing fiber. $\lambda/4$: quarter-wave plate. Pol.: polarizer. The points A, B, C, D, and E identify characterization locations.

data streams are coded by electroabsorption modulators, one for each channel, in the hybridized circuit.

The data stream of 1-ps pulses, with 6.25-ps spacing, is amplified and transmitted through a DM fiber channel to the unique nonlinear optical waveguide receiver. All-optical demultiplexing is accomplished via a $\chi^{(2)}$ interaction between the data pulses, operating at the system rate, and a counter-propagating timing pulse, operating at the channel rate. The collisions between timing pulses and data pulses produce second-harmonic signals that propagate normal to the waveguide surface, thus generating a parallel set of data streams spatially separated along the demultiplexer waveguide. Importantly, a single timing pulse demultiplexes multiple data pulses in a single operation without added complexity. Thus, all-optical serial-to-parallel (S/P) conversion is accomplished at high data rates without requiring ultrafast electronics; indeed, only 10-Gb/s electronics are necessary. The timing pulse is locally generated at the channel rate via a second picosecond-pulse source, which is synchronized with the data stream following signal detection and clock recovery.

Here, we review our recent efforts with respect to the short-pulse source (Section II), the hybrid modulator/multiplexer with integral spot-size converters (SSCs) (Section III), and the dispersion- managed fiber channel (Section IV). Furthermore, we focus on the unique all-optical demultiplexer (Section V), and report bit error rate (BER) measurements for channel rates of 2.5 Gb/s enabled by a microcavity resonator to enhance the nonlinear interaction in the AlGaAs demultiplexer waveguide. The described experimental results are mostly performed at 2.5 Gb/s due only to available receiver technology at the detection wavelength of $\sim$775 nm; however, as discussed, each of the components is easily scaleable to 10 Gb/s. Our development efforts for 10-Gb/s, 775-nm receivers are also discussed in Section VI.

II. Picosecond-Pulse Source

The performance of a return-to-zero (RZ) optical data link depends strongly on the initial pulse quality. The picosecond-pulse source (psPS) (Fig. 2) provides the channel-rate (10-GHz) stream of picosecond pulses that exhibits the features needed for the OTDM link. In this section, we describe our experimental results obtained from a four-stage source that produces picosecond and sub-picosecond pulses at multi-GHz rates. The system is compact, robust, and easily scalable to repetition rates of 10 GHz and higher. The results presented here are obtained from a 2.5-GHz implementation.

A. Gain-Switched Laser Diode

Stage 1 of the psPS is a distributed-feedback (DFB) laser diode (LD) gain-switched (GS) in the conventional manner: the rising edge of the sinusoidal drive current initiates a series of relaxation oscillations in the LD output and the falling edge truncates the series after the first peak. The resulting pulse is much shorter than the sinusoidal period. Importantly, the optical pulse exhibits a strong, nearly linear, negative chirp due to the dependence of the refractive index on carrier density.

The output of Stage 1 (Point A in Fig. 2) is characterized by a full-width at half-maximum (FWHM) temporal width of $\Delta t = 18$ ps (assuming a Gaussian shape) and an autocorrelation peak-to-pedestal ratio of $R_{pp} = 24$ dB (Fig. 3). The spectral FWHM is $\Delta\lambda_{\mathrm{FWHM}} = 0.54$ nm, corresponding to a time-bandwidth product (TBP) of 1.2, which is consistent with a strongly chirped pulse. In the OTDM link described here, the timing jitter of the source must be much less than the 6.25-ps bit period. Measurements performed in the time domain with a 40-GHz sampling oscilloscope and in the frequency domain with an RF spectrum analyzer [7] yield an rms timing jitter of $\sigma_J = 970$ fs. Furthermore, pulse jitter generally scales inversely with drive frequency, and thus improved performance is expected for operation at 10 Gb/s. The remaining stages of the psPS do not significantly affect jitter.

B. Linear Pulse Compressor

Stage 2 is a linear pulse compressor [8]–[11] consisting of 200 m of dispersion-compensating fiber (DCF), characterized by positive (normal) dispersion with a dispersion parameter of $D = -92$ ps/(nm–km). Thus, by appropriate choice of DCF length, the linear component of negative chirp of the pulse is compensated. At the output of Stage 2 (Point B in Fig. 2), the pulse width is reduced to 8.3 ps (assuming a Gaussian shape), and R_{pp} is reduced to 20 dB due to imperfect compression. Similar to Stage 1, $\Delta\lambda_{\mathrm{FWHM}} = 0.53$ although the TBP is only reduced to 0.70. We note that we have optimized the LD drive parameters for best overall pulse characteristics at Stage 4, and therefore the Stage 2 performance may not be optimal.

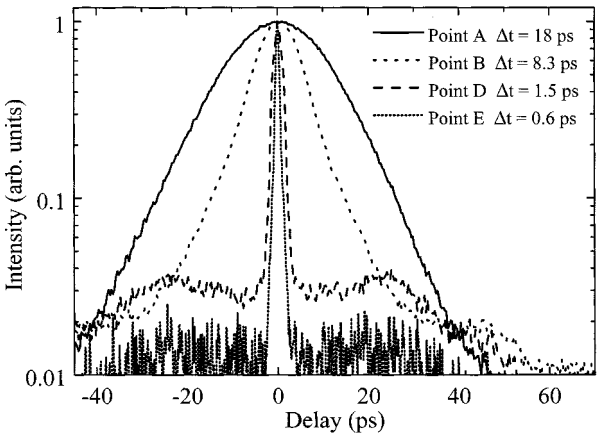

Fig. 3. Optical pulse autocorrelations measured at Points A, B, D, and E. The pulse widths at Points A and B were calculated assuming a Gaussian shape. The pulse widths at Points D and E were calculated assuming a sech^2 shape.

C. Adiabatic Pulse Compressor

Stage 3 is an adiabatic pulse compressor [12], [13] composed of an erbium-doped fiber amplifier (EDFA) followed by a length of dispersion-decreasing fiber (DDF). DDF exhibits negative (anomalous) dispersion that decreases in magnitude along the length of the fiber. The DDF has a length of $L_{\mathrm{DDF}} = 11$ km, with an initial dispersion parameter of $D(0) = 10.5$ ps/(nm–km) and a final dispersion parameter of $D(L_{\mathrm{DDF}}) = -0.1$ ps/(nm–km). The EDFA provides the energy required for the pulse to form a fundamental soliton in the DDF. Subsequently, the soliton experiences decreasing dispersion as it propagates and thus shortens to maintain soliton order.

The output of Stage 3 (Point D in Fig. 2) is characterized by a pulse width of 1.5 ps (assuming a sech^2 shape) and a broad pedestal ($R_{pp} = 14$ dB) in the autocorrelation (Fig. 3), due to imperfect compression. A sech^2 shape is assumed since any nonsoliton energy should dissipate as the pulse propagates through the DDF. Because of the CW component in the spectrum ($\Delta\lambda_{\mathrm{FWHM}} = 0.52$), the rms spectral width, $\Delta\lambda_{\mathrm{rms}} = 4.22$ nm, is a better measure of spectral content; using $\Delta\lambda_{\mathrm{rms}}$ to calculate the TBP yields 0.79.

D. Artificial Saturable Absorber

Stage 4 is an artificial saturable absorber created by combining nonlinear polarization rotation in the DDF, which creates an intensity-dependent elliptically polarized beam, with polarization filtering provided by a quarter-wave $(\lambda/4)$ plate and a polarizer. The $\lambda/4$ plate is oriented to transform the polarization of the peak intensity to a linear polarization; the polarization of the wings remains in an elliptical state. Subsequently, the polarizer selects the peak and rejects the portion of the wings that are orthogonally polarized. The output of Stage 4 (Point E in Fig. 2) is characterized by a pulse width of 0.6 ps (assuming a sech^2 shape) and an increased $R_{pp} = 17$ dB. $\Delta\lambda_{\mathrm{rms}} = 4.5$ nm and the TBP is 0.32, indicating that the pulse is nearly transform-limited.

The psPS produces pulses as short as 0.60 ps at a 2.5-GHz rate with a jitter of 970 fs. Operation at 10 GHz is expected to both decrease the jitter by a factor of four and improve the performance of the linear compressor. Thus, we have demonstrated a compact method for the production of short pulses at high repetition rates with sub-picosecond jitter.

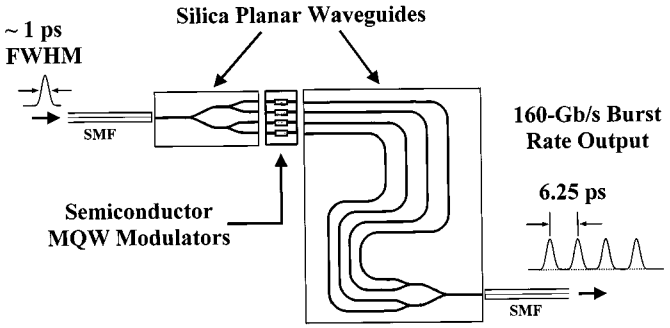

Fig. 4. Integrated-optical temporal multiplexer. Silica planar waveguides form the 1 : 4 splitter and the delay line/1 : 4 recombiner. The array of semiconductor MQW electroabsorption modulators has integral SSCs for matching to the mode size of the silica waveguides.

III. Optical Modulation and Multiplexing

Temporal multiplexing of 16 10-Gb/s channels into one 160-Gb/s pulse stream can be performed via a hybrid assembly (Fig. 4) of integrated-optical components, including silica 1-by-4 splitters, arrays of electroabsorption modulators with integral SSCs, and silica delay line/4-by-1 recombiners [14]. The silica components are fabricated using a planar waveguide process. Here we describe a four-bit implementation of the multiplexer that operates at a burst rate of 160 Gb/s and is scalable to the full 16 bits.

The hybrid multiplexer performs two major functions. First, it generates a sequence of pulses by splitting, differentially delaying, and recombining an input pulse sequence. Second, the multiplexer encodes data on each of these pulses via electroabsorption modulators that are integrated into each pulse path before recombination of the pulses. Consequently, silica waveguides and travelling-wave semiconductor devices can be integrated in a hybrid manner to construct a compact integrated-optical signal-processing device, which we refer to as the IOTM. This hybrid approach allows both the semiconductor and silica materials to be exploited to full advantage.

A. Silica Integrated-Optical Temporal Multiplexer

The IOTM uses buried silica-on-silica waveguides that have been fabricated with an index contrast of 0.75%. The IOTM splits the input pulse stream provided by the picosecond-pulse source via concatenated Y-junctions. Data is encoded onto each of these individual pulse streams via an array of electroabsorption modulators. Each stream is then differentially delayed and subsequently recombined to generate the system-rate 160-Gb/s data stream.

The temporal response of a silica splitter/delay/recombiner fabricated without modulators was characterized directly in the time domain as well as indirectly using a frequency-domain technique. In the time domain, a nonlinear cross-correlation measurement was performed using an optical parametric oscillator with a 150-fs FWHM pulse. In the frequency domain,

spectral interference yields a modulated power spectrum that reveals the temporal pulse separation via Fourier analysis [15]. The direct and indirect measurements of the temporal response of the splitter/delay/recombiner are in good agreement and confirm the required amplitude uniformity and 6.25-ps pulse separation.

B. Electroabsorption Modulators

The switching elements in the IOTM are strained InGaAs/InAlAs multiple-quantum-well (MQW) p-i-n electroabsorption (EA) modulators. Similar EA modulators have been demonstrated with fast ($>$ 20 GHz) optical responses and large extinction ratios [16]. The EA modulators used for the IOTM are designed for polarization insensitivity, low bias, and high speed. We have successfully demonstrated efficient, polarization-insensitive modulators with a 25-dB extinction ratio for a 4-V drive voltage [17].

The modulator structure is a p-i (MQW)-n diode. The intrinsic region consists of ten 50-Å $In_{0.60}Al_{0.40}As$ barriers with ten 120-Å $In_{0.47}Ga_{0.53}As$ wells. The p-type region is Be-doped $In_{0.52}Al_{0.48}As$ and the n-type region is n^+-InP. The 0.5% tensile strain in the MQW region provides the polarization insensitivity in the modulator [18]. Electrical and optical tests of the EA modulators demonstrate that the fabricated devices satisfy the low-bias and high-speed requirements for the IOTM. The capacitance-limited bandwidth for 500-μm modulators is 6 Gb/s, and thus 10-Gb/s operation is anticipated for 250-μm devices.

C. Integrated Spot-Size Converters

The problem of spot-size mismatch between the silica and semiconductor waveguides can be solved using integrated SSCs. Large passive mesa waveguides are incorporated into the semiconductor structure to enable efficient coupling to the optical modes of fibers or similar silica waveguides. The mesa waveguides also efficiently transfer optical power to the active waveguide, which typically has a much smaller mode size. This approach [19] is highly attractive in that no regrowth steps are required, and the entire SSC-p-i-n-SSC device can be fabricated by standard lithographic and etching techniques [20]–[22]. Power transfer from the larger passive waveguide, which is typically located between the substrate and the active waveguide (Fig. 5), is accomplished by a combination of resonant and adiabatic coupling. The ridge that defines the upper active p-i-n waveguide is tapered in the transverse direction, reaching zero width before the ends of the device. At the input and output facets of the device, the upper p-i-n waveguide is at cutoff, and the field propagates exclusively in the passive mesa waveguide. Away from the input facet, the effective index of the tapered waveguide increases with the width of the waveguide ridge until, at some location upstream from the input, phase matching occurs between the mesa and the p-i-n waveguide. The field is evanescently coupled to the p-i-n waveguide, with almost complete power transfer. The optical pulses are modulated and then propagate toward the SSC at the output end, where the power is transferred back into the larger mesa waveguide by means of the corresponding output taper of the p-i-n waveguide.

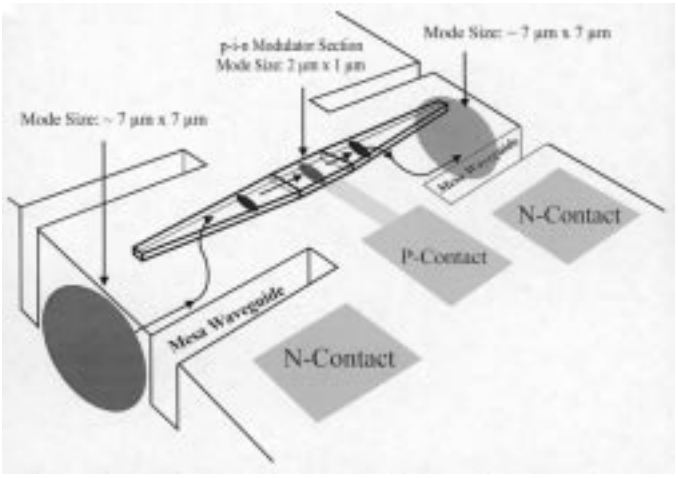

Fig. 5. Multiple-quantum-well p-i-n modulator with integral SSCs. The tapered waveguide of the modulator allows for coupling of the power from the lower mesa waveguide to the modulator and back to the mesa waveguide. The RF signal is applied through the p-contact.

The SSC-p-i-n-SSC structure is advantageous in several respects. First, the integrated SSCs allow the effective length of the modulator structure to be 250 μm without being difficult to handle. Second, the monolithic design allows nearly independent optimization of the p-i-n modulator structure and the SSC structure. The fabricated SSCs described here also incorporate a passive mesa waveguide that is discontinuous to enhance the extinction ratio of the p-i-n modulator. Specifically, the mesa waveguide does not have lateral confinement along the entire length of the device. Thus, any power not coupled from the mesa waveguide to the p-i-n modulator is severely attenuated before reaching the output mesa waveguide through the intermediate slab located beneath the active section of the p-i-n waveguide. Simulations reveal a contrast enhancement of 4 dB for the discontinuous waveguide. Furthermore, the spot-size conversion is achieved with a large taper tip width of 1.2 μm, obviating more challenging sub-micron lithography and increasing the yield for the arrays of SSC-p-i-n-SSC modulators required for the IOTM.

Fabricated SSC structures are shown in Fig. 6. The epistructure was grown by molecular beam epitaxy, and device fabrication involves standard contact lithography and dry etching. The width of the mesa waveguide is 9 μm, whereas that of the p-i-n waveguide is 3 μm. The mesa waveguide is etched to a depth of 5 μm, and the p-i-n waveguide is etched to a depth of less than 2 μm. The length of the p-i-n waveguide is 250 μm, with 250-μm tapers at its input and output. The overall length of the SSC-p-i-n-SSC device is less than 1000 μm. The salient features of the etched waveguides are the smoothness and straightness of the sidewalls and the relatively large tip dimension of $>$1.0 μm.

The expected total insertion loss of an optimized SSC device is less than 10 dB. For simplicity, initial testing of the SSC-p-i-n-SSC modulator structure was carried out with cleaved DSFs in place of the silica waveguides. The larger mode-size of the 0.75%-silica waveguides results in increased coupling loss. The measured insertion loss for a typical cleaved device was $\sim$20 dB when coupled to DSF. Our measurements of lensed-fiber coupling to a nearly identical p-i-n modulator waveguide yielded an insertion loss of 10 dB. Accounting

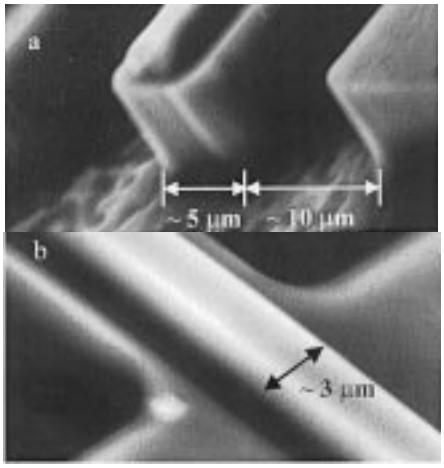

Fig. 6. Scanning electron micrographs of the fabricated p-i-n modulator structure with SSCs. (a) The structure at a cleaved plane. (b) The modulator waveguide, demonstrating smooth sidewalls, and the trenches used to define the mesa waveguide.

then for the known absorption loss and estimated Fresnel and mode-mismatch losses, we estimate that an optimized structure coupled to silica waveguides will yield a total insertion loss of less than 9 dB. The optimized structure includes a thicker mesa waveguide as well as antireflection-coated facets. We note that the insertion loss of a 250-μm modulator waveguide without SSCs is estimated to be 25 dB when coupled to a silica waveguide of the IOTM; the margin of improvement for a p-i-n modulator with SSCs over a p-i-n modulator alone is therefore approximately 15 dB.

IV. Short-Pulse Propagation

The transmission integrity of short pulses can be enhanced by the use of the nonlinearity in optical fiber, as is the case with DM solitons. Indeed, transmission over tens of thousands of kilometers is possible when optical solitons are combined with active in-line control. However, true first-order-soliton propagation of 1.0-ps FWHM pulses is limited to approximately 100 km and requires DSF [3]. Thus, variations of soliton propagation, such as with DM solitons [23]–[25] and adiabatic soliton propagation [23] have enabled the extension of propagation distances for short pulses. The following sections describe the use of DM solitons within our RZ, 160-Gb/s system, including the limitations associated with polarization-mode dispersion (PMD).

A. Dispersion-Managed-Soliton Propagation

In systems using DM solitons, the transmission fiber consists of alternating segments of normal- and anomalous-dispersion fibers, typically designed to yield slightly anomalous net dispersion. Dispersion maps with net normal dispersion have been demonstrated [23]; however, these spans are difficult to implement in practice. In the case of first-order solitons, the nonlinear phase shift due to self-phase modulation balances the dispersion. Stable propagation is enabled using DM solitons in the presence of a small amount of net anomalous dispersion. This stability may be viewed as a locally linear process where the pulse dynamics are dictated by the dispersion in the individual segments; however, a small amount of nonlinearity is sufficient to balance the residual anomalous dispersion [25]. Due to these alternating segments of fiber, DM solitons are advantageous over pure soliton transmission. First, DM solitons reduce the cumulative dispersion, which allows for an increased, yet distributed, energy per pulse [24]. Second, DM solitons exhibit less noise- and timing-induced jitter due to the low average dispersion and high local dispersion [24]. Third, DM solitons are more robust in the presence of power fluctuations.

B. Polarization-Mode Dispersion

PMD may the limiting factor in 160-Gb/s transmission systems. PMD acts on the orthogonal polarizations of the pulse, causing them to propagate at different group velocities in the fiber. The time-averaged differential group delay (DGD) is $\langle \mathrm{DGD} \rangle = \mathrm{PMD}\sqrt{z}$, where the PMD coefficient is in units of ps/$\sqrt{\mathrm{km}}$ for the strong-mode-coupling case. PMD is stochastic in nature, and therefore the amount of DGD will vary on a time scale of minutes due to variations in the fiber environment. Thus, the PMD coefficient does not anticipate the worst-case degradation in the signal. Our 1.0-ps RZ pulses may broaden to NRZ pulses after approximately 2750 km in typical modern fiber, where the PMD coefficient is less than 0.1 ps/$\sqrt{\mathrm{km}}$. PMD may limit our ability to maintain an RZ format with a maximum duty factor of 33%, which results in a transmission length of approximately 100 km.

C. Link Design

We have investigated two separate approaches, one employing linear propagation techniques and the other DM solitons. For the latter case, the dispersion map consists of 50 km of a nonzero dispersion-shifted fiber (NZDSF) (Corning LEAF+) with a dispersion parameter of $D = 5.0$ ps/(nm–km) and 49.8 km of fiber with a dispersion parameter of -5.0 ps/(nm–km) (Corning Submarine LS+). Previously, standard-effective-area NZDSF enabled 1.8-ps pulses to be transmitted over 300 km in a quasi-linear transmission configuration [26]. Using linear propagation techniques, whereby the link is strongly optical-SNR-limited, the pulse energies are such that the dispersion length is much greater than the nonlinear length ($L_D \gg L_{NL}$) [23] and the path-averaged dispersion of the channel is set to zero. In the nonlinear DM soliton propagation regime, a net anomalous dispersion parameter of 0.01 ps/(nm–km) ensures that our span length of 100 km is slightly less than the soliton period in order to enable DM soliton propagation. This design will allow the assessment of 160-Gb/s transmission of 1.0-ps pulses through 100 km of NZDSF where the pulses are maintained through a semi-linear soliton process.

V. Surface-Emitted Second-Harmonic Demultiplexer

An all-optical S/P converter [17], [27] based on SESHG in optical waveguides can serve as a demultiplexer in a high-capacity OTDM system. The surface-emitting geometry [28] differs from the more common collinear SHG geometry in that counter-propagating fundamental beams are required, and the resulting harmonic propagates normal to the direction of the two fundamental beams. Thus, for fundamental light propagating

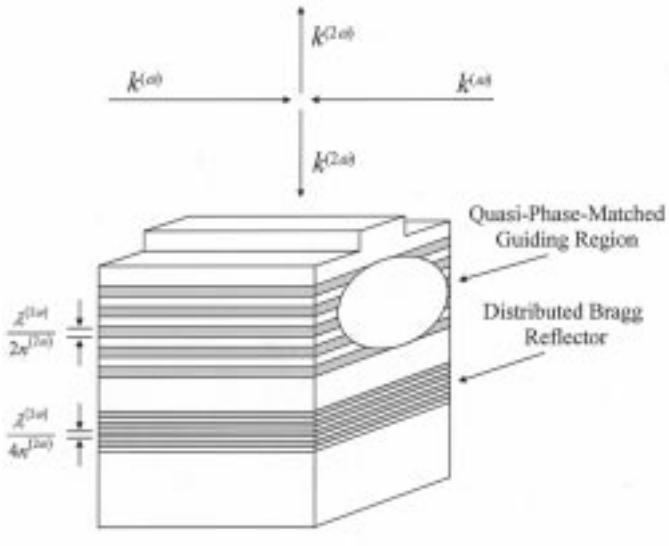

Fig. 7. SESHG in a quasi-phase-matched multilayer channel waveguide. A DBR is incorporated beneath the waveguide core to reflect the downward-propagating portion of the second harmonic back toward the surface.

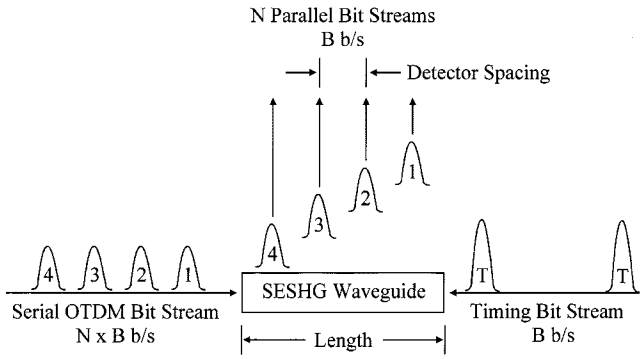

Fig. 8. Optical S/P converter. N channels are demultiplexed down to B bits per second each. The required waveguide length is determined by B, while the detector spacing is determined by $N \times B$. A 4-channel implementation is shown.

in a vertically quasi-phase-matched waveguide with the appropriate crystal orientation, the enhanced harmonic will propagate toward both the surface and the substrate (Fig. 7). Symmetry requires equal amounts of SH to be radiated both up and down; the incorporation of a distributed Bragg reflector (DBR) beneath the waveguide core allows the downward-propagating portion to be reflected back toward the surface. Devices are fabricated using $Al_xGa_{1-x}As$, which allows exploitation of the large $\chi^{(2)}$ of this system while simultaneously tailoring the band gap to minimize the optical absorption in the DBR and the quasi-phase-matched waveguide core. In this section, we describe the operation of the S/P converter and discuss methods to enhance the conversion efficiency.

A. Device Description

Operation of the SESHG S/P converter is shown in Fig. 8. The OTDM data stream and a locally generated timing pulse are coupled into opposite ends of the SESHG waveguide. The timing pulse operates at the channel rate (e.g., 10 Gb/s) and interacts with each oncoming data pulse, generating a second-harmonic signal that is emitted toward the top surface of the waveguide. Since these interactions occur at different spatial locations, the second-harmonic signals from the different data bits are distributed along the length of the waveguide. Thus, a temporal-to-spatial mapping is performed, generating separate parallel bit streams at the channel rate from a single serial stream at the system rate. The second-harmonic signals can then be collected by an array of appropriately positioned optical fibers, with each fiber routed to a separate photodetector with a bandwidth sufficient to detect data at the channel rate. Ultimately, the optical fibers collecting the SH can be replaced with a flip-chip detector array integrated with receiver electronics in order to create a more compact device. The number of channels that can be demultiplexed is determined by the number of interactions allowed in the nonlinear waveguide, and is limited only by practical considerations of material uniformity and absorptive/scattering loss of the fundamental power since conversion depletion of the fundamental is negligible.

As an alternative to generating the timing bit at the demultiplexer, the timing pulse can be generated in the IOTM and transmitted with the data stream, enabling self-timed operation [27], [29]. The counter-propagating timing pulse is then obtained by reflecting the combined data/timing pulse stream from the rear facet of the waveguide. When the timing pulse precedes the first data pulse by 1.5 data-pulse intervals, the data-data collisions are centered between adjacent timing-pulse/data-pulse collisions. In this self-timed scheme, the second harmonic is collected in the usual fashion with minimal crosstalk from the data-data collisions.

The SESHG S/P converter has several advantages over other OTDM demultiplexing schemes. First and most important, it allows the recovery of all multiplexed channels with a single operation within a single device. Demultiplexers based on interferometric switching [30]–[33] typically require an individual device for each OTDM channel. Other techniques are capable of multiple-channel operation, but require precision control of the dispersion [34] or precise timing between multiple complex components [35], [36]. Second, the S/P converter requires only one timing pulse, whereas the interferometric techniques typically employ a separate, precision-timed pulse source for each channel that is to be demultiplexed. Third, the S/P converter has a significant advantage in terms of simplicity. The semiconductor growth is similar to that of a standard vertical-cavity surface-emitting laser; fabrication is straightforward, requiring no complicated semiconductor regrowth, no electrical contacts, and only one photolithographic mask and etch. In contrast, integration of multiple single-channel interferometric demultiplexers on one die is complex and subject to strict fabrication tolerances. Finally, this scheme is highly compact and compatible with semiconductor integration, resulting in a conveniently packaged device.

The basic functionality of the S/P converter has been demonstrated [29]; however, the conversion efficiency is limited by the short interaction lengths of the colliding-pulse geometry. Several methods have been proposed to improve the efficiency of the SESHG process. Normandin *et al.* demonstrated that a

quasi-phase-matching (QPM) condition can be achieved by using a multilayer waveguide core with alternating regions of high and low $\chi^{(2)}$ [37]. This arrangement allows significant constructive addition of the vertically propagating second harmonic. QPM provides an enhancement of several orders of magnitude compared with a bulk waveguide of the same core thickness ($\sim$1 μm).

Further enhancement can be obtained using alternate crystal orientations. Most SESHG work has been performed with [100]-oriented material, although this orientation is not optimal and requires both TE and TM polarizations in the counter-propagating beams. Indeed, an enhancement of 8/3 in the SESHG power integrated along the length of the waveguide can be obtained using either [110]- or [211]-oriented material. Furthermore, only TE excitation [38], [39] is required. These two orientations can provide the same optimum efficiency, but the [211] orientation is preferred because the propagation direction with optimum efficiency allows the waveguide facets to be defined simply by cleaving the semiconductor sample.

An additional method to improve SESHG efficiency, resonant-cavity enhancement (RCE), has also been investigated [40]–[44]. However, the effects of short pulses and the commensurate broad spectral content, as required for >100-Gb/s operation, have not been previously explored. RCE has been used in this work to improve the efficiency by more than an order of magnitude for 1-ps pulses, as verified by direct comparison to non-RCE devices.

B. Efficiency and Resonant-Cavity Enhancement

The conversion efficiency in SESHG waveguides is characterized by a nonlinear cross section parameter A^{NL} [45]

$$\frac{P^{(2\omega)}}{l \cdot w} = A^{NL} \frac{P_+^{(\omega)}}{w} \frac{P_-^{(\omega)}}{w}. \tag{1}$$

Here, $P^{(2\omega)}$ is the SH power, $P_+^{(\omega)}$ and $P_-^{(\omega)}$ are the counter-propagating fundamental powers, l is the interaction length defined by the overlapping pulses, and w is the effective width of the waveguide [46]. Reported values for the nonlinear cross section vary, but a typical value for the preliminary QPM GaAs-based SESHG waveguides without RCE discussed below is $8.7 \times 10^{-8} W^{-1}$. This implies that an 8-pJ timing pulse within a 4-μm wide waveguide yields an energy efficiency of $E_{SH}/E_{data} \sim 10^{-5}$.

For comparison, the nonlinear cross section required for a 160-Gb/s demultiplexer operating with 16 10-Gb/s channels can be estimated. Such a device is 5 mm long, with the demultiplexed channels spaced by approximately 280 μm. The maximum attainable input power is determined both by available power from an optical preamplifier and by facet damage thresholds. Limiting the average power incident on each facet to 160 mW, assuming coupling and propagation losses of 3 dB or less, and assuming half of the data bits are "ones", we arrive at an 8-pJ timing pulse and 1-pJ data pulses at the interaction locations inside the waveguide. The required nonlinear cross section is listed in Table I for a number of receiver sensitivities assuming a typical effective waveguide width of 4 μm. Note that the required A^{NL} or receiver sensitivity scales linearly with the energy of the timing or data pulse. Assuming optimized receivers in the target sensitivity range of -20 to -26 dBm, the nonlinear cross section must be enhanced by nearly two orders of magnitude as compared to the measured value in the preliminary [100] GaAs-based waveguides.

TABLE I
NONLINEAR CROSS-SECTION REQUIRED FOR VARIOUS RECEIVER SENSITIVITIES

Assuming 1-pJ Data Pulse, 8-pJ Timing Pulse, and 4-μm Mode Width	
10-Gb/s Sensitivity at 775 nm	**Required A^{NL}**
-20 dBm	2.0×10^{-5} W^{-1}
-23 dBm	1.0×10^{-5} W^{-1}
-26 dBm	5.0×10^{-6} W^{-1}

A theoretical assessment of a vertical cavity resonant at 2ω reveals a dramatic enhancement in the SH conversion efficiency, as well as a dependence on the spectral content. Specifically, an enhancement of $\sim$30 is possible for 1-ps fundamental pulses. This, combined with the enhancement from the [211] orientation, should be sufficient to achieve the performance cited in Table I. By correctly positioning DBRs above and below the waveguide core, the majority of the SH is folded back upon the interacting fundamental pulses in a coherent fashion. Thus, the resonant cavity effectively increases the interaction length, which would otherwise be fixed by the pulse widths in the counter-propagating geometry.

Beginning with the methods of [39] and [47], we find the frequency-dependent SH resonant enhancement to be

$$\frac{P_t^{(2\omega)}}{P_o^{(2\omega)}} = \frac{\left(1-|r_t|^2\right)\left(1+|r_b|\exp(-\alpha d/2)\right)^2}{\left(1-|r_t|\,|r_b|\exp(-\alpha d)\right)^2+4|r_t|\,|r_b|\exp(-\alpha d)\sin^2\theta/2} \tag{2}$$

where

$P_t^{(2\omega)}$	SH power transmitted through the top mirror;
$P_o^{(2\omega)}$	SH power generated in one direction in the absence of the resonator;
r_t and r_b	top and bottom SH field reflectivities;
α	average power absorption coefficient for a single pass through the cavity;
d	mirror separation;
Θ	round-trip phase shift in the cavity.

The round-trip phase shift includes the penetration depth into the Bragg reflectors [48], which can be large for low-index-contrast mirrors. The frequency dependence of the enhancement is incorporated through the $\sin^2\theta/2$ term, which is neglected for a quasi--CW resonance. The SH source is treated as a lumped element located at the center of the cavity. The lower DBR is optimally positioned for coherent reflection of the SH, providing up to a factor of four enhancement when the top DBR reflectance is zero. The enhanced SH power spectrum is obtained from the product of the enhancement factor in (2) and the nonenhanced

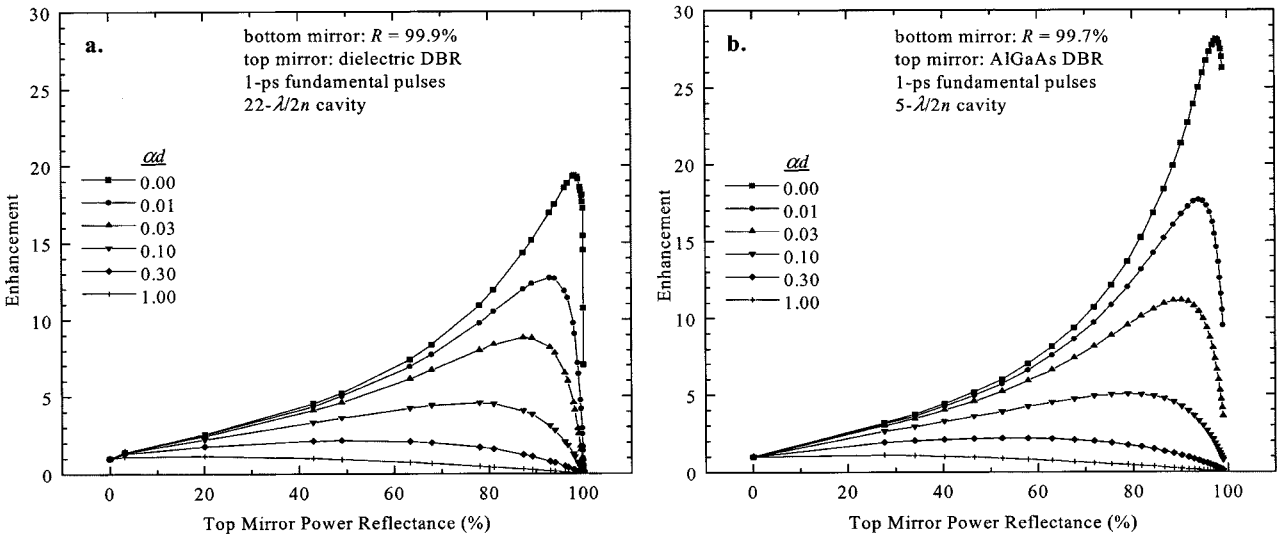

Fig. 9. Calculated resonant enhancement of second-harmonic power as a function of top mirror reflectance for 1-ps fundamental pulses in (a) a 22-$\lambda/2n$ cavity, and (b) a 5-$\lambda/2n$ cavity. The single-pass cavity loss is given by αd. All results are normalized to the power with a top reflectance of zero, and thus the enhancement is relative to the case where only the lower mirror is present.

power spectrum $P_o^{(2\omega)}$, and the net enhancement is found by integrating the enhanced and nonenhanced spectra over frequency. We note that (2) is independent of chirp, and thus it is the magnitude of the spectral content of the data and timing pulses that determines the performance.

The microcavity can be sufficiently small that multiple round trips of the SH occur during the overlap of the colliding fundamental pulses, increasing the intensity of the SH signal. In a $d \approx 2$-μm cavity, multiple round trips occur even for 1-ps fundamental pulses. For realizable structures, a careful optimization of the cavity parameters is necessary to maximize performance. These parameters include the absorption and scattering losses present in practical structures, the fraction of light lost through the bottom DBR, the size of the cavity, and the content of the nonenhanced SH power spectrum.

We have implemented a numerical optimization based on (2) for 1-ps, 1.55-μm Gaussian fundamental pulses by varying only the top mirror reflectance. The lower mirror is an AlGaAs DBR with a power reflectance of $>99\%$ so that most of the SH is emitted through the top mirror rather than into the substrate. The number of top DBR layers is varied for given values of the attenuation. For simplicity, we have assumed that the refractive index and $\chi^{(2)}$ are constant over the small bandwidth considered. Results are shown in Fig. 9(a) for a dielectric top DBR and a mirror separation $d = 22\lambda^{SH}/2n$, where n is the refractive index. Results are also shown for a smaller cavity with an AlGaAs top DBR and $d = 5\lambda^{SH}/2n$ in Fig. 9(b). The results are normalized to the case where $r_t = 0$ for comparison to waveguides with a top antireflection (AR) layer, and thus the total enhancement due to the cavity is up to a factor of four larger than depicted.

Several trends are evident in Fig. 9. For a given cavity finesse (i.e., fixed mirror reflectances), the enhancement is larger for a smaller cavity, since reducing the mirror separation increases the spectral width of the resonance. The large penetration depth in the low-contrast AlGaAs DBRs therefore presents a limitation; for the small-cavity structure with AlGaAs DBRs in Fig. 9(b), the penetration depth is comparable to the mirror separation. Clearly, structures with higher confinement, e.g., those employing selectively oxidized AlGaAs/Al_2O_3 DBRs [44], can result in larger enhancements. The optimum value of top mirror reflectance also decreases as the cavity absorption increases, since the SH experiences more loss as it makes more round trips in a cavity with higher reflectance. The cavity becomes detrimental when the absorption length is comparable to the mirror separation d, and thus minimization of absorption is critical to efficient performance.

C. Device Fabrication and Characterization

The $Al_xGa_{1-x}As$ system provides a convenient set of lattice-matched alloys where the nonlinearity can be easily modulated by up to an order of magnitude through control of the aluminum fraction. Vertically quasi-phase-matched structures and DBRs can be readily grown using standard epitaxial techniques such as molecular-beam epitaxy (MBE) or metal-organic chemical-vapor deposition.

Initial [100] waveguides characterized in this work utilized GaAs for the high-$\chi^{(2)}$ layers. The bandgap of GaAs is less than the SH photon energy, resulting in linear absorption of the second harmonic and also two-photon absorption (TPA) of the fundamental. To eliminate these losses and other deleterious effects associated with TPA-induced carriers [49], the GaAs layers have been replaced with $Al_{0.32}Ga_{0.68}As$ in recent devices. Additional performance enhancement is provided by a [211]-oriented MBE growth of the AlGaAs structure, including the lower DBR, the $Al_{0.90}Ga_{0.10}As$ cladding layers, and the 9-layer $Al_{0.32}Ga_{0.68}As/Al_{0.90}Ga_{0.10}As$ QPM core. Channel waveguides are formed by etching ribs of various widths and depths into the upper cladding layer via standard photolithography and reactive-ion etching. Alternating layers of SiO_2 and Si_3N_4 are then deposited using plasma-enhanced chemical-vapor deposition to form the dielectric top DBR.

The SESHG efficiency has been characterized in the new [211] AlGaAs structures both with and without the top DBR. The nonlinear cross section is measured using the rear-facet reflection geometry, where a single fundamental pulse is allowed to propagate down the entire length of the guide. The ~30% Fresnel reflection from the semiconductor-air interface at the rear waveguide facet creates a counter-propagating fundamental. The SH is collected with a high-numerical-aperture (NA), wide-core optical fiber and measured with a calibrated avalanche photodetector. The fundamental power transmitted though the waveguide is focused onto a second calibrated photodetector using a high-NA, AR-coated microscope objective. The nonlinear cross section is then calculated using (1). Nonlinear cross section values for initial [211]-oriented $Al_{0.32}Ga_{0.68}As$-based structures have been measured to be $\sim 2 \times 10^{-7}$ W^{-1} without the top DBR, and $\sim 2 \times 10^{-6}$ W^{-1} for a 1-ps pulse and a nonoptimal top DBR reflectance of 77%. This microcavity A^{NL} represents an improvement of a factor of ~ 25 over the original nonenhanced [100] GaAs-based SESHG waveguides, and is within a factor of two of the target efficiency for 160-Gb/s operation cited in Table I. Additional improvement is possible with optimization of the resonant cavity structure for 1-ps pulses.

VI. Optical Receiver

The short optical pulses generated by the all-optical demultiplexing require high sensitivity 775-nm receivers capable of 10-Gb/s performance. While the requirements are difficult to meet, the RZ data format provides opportunities to enhance receiver performance in ways not available in NRZ systems [50], [51]. Here we describe our design considerations for a 10-Gb/s, 775-nm receiver. For the purpose of relating BER performance to receiver characteristics, the expression for the well-known Q-factor is stated in terms of parameters such as receiver bandwidth B and rms noise voltage generated in the electronics. By making the usual assumptions on the statistical nature of these parameters, we can relate the Q-factor to BER. The direct analysis presented here is used to identify the minimum performance level of the receiver.

A. Signal Response

If we assume that the entire system has a low-pass response, then we can determine the output signal peak-to-peak amplitude, $V_{p\text{-}p}$, from the receiver impulse response. For simplification, we can distill the two scalar terms, detector responsivity $\Re$, and amplifier transimpedance Z_t, and combine the spectral response of each component into a normalized system impulse response. If we assume that the optical pulse is impulse-like (relative to receiver bandwidth) with pulse energy, E, the amplitude of the temporal voltage can be easily determined

$$V_{p\text{-}p} = \eta EB \cdot \Re Z_t \tag{3}$$

where η is a scaling factor to account for the shape of the impulse response [50], [52]. We note that while (3) is obvious, the ramifications may not be. Within the aforementioned conditions, if the bandwidth of the electronics is increased, the amplitude of the output voltage will increase proportionally. In RZ systems, the effective optical power (ηEB) is a function of the receiver, whereas in the NRZ systems it is not necessarily influenced by the receiver performance.

B. Electronic Noise and Q-Factor

For noise consideration, we must take into account the methods of signal enhancement. We first consider transistor-based amplification where thermally generated noise, specified as input-referred spectral-density current i_{th} dominates. Under this condition, the rms noise voltage will be independent of signal voltage, and the resulting approximation for Q-factor is

$$Q = \frac{\Re E \eta \sqrt{B}}{2 i_{th}}. \tag{4}$$

Since the signal amplitude is directly proportional to B and the noise voltage is proportional to $B^{1/2}$, increasing the receiver bandwidth can enhance the Q-factor.

Next, we consider the case where receiver sensitivity is paramount and avalanche multiplication is used. In this case, performance will be dominated by shot noise that occurs in the opto-electronic conversion process. This noise is signal-dependent $(\sigma^2 = 2qI)$, and as a result, the Q-factor can be approximated as

$$Q = \sqrt{\frac{\Re \eta E}{2 q F_e}} \tag{5}$$

where F_e is the excess noise factor of the detectors. Because both signal and noise are dependent on B, the Q-factor remains unaffected by the increased bandwidth.

It is now evident how the RZ data format can be exploited for enhancing sensitivity. By increasing the bandwidth in an RZ system, the Q-factor increases (or at least remains unchanged), whereas in an NRZ system the increased bandwidth serves only to increase noise without benefit to the signal amplitude. Again, the analysis presented here considers only the electronic noise and is only useful to determine an upper bound of the receiver performance. The full impact of factors such as amplified spontaneous emission, relative intensity noise, crosstalk, and the nonlinear demultiplexer have not been thoroughly explored. Indeed, the analysis in [53] shows that the influence of optical noise on the BER may vary significantly based on factors such as A^{NL}, the ratio of $P_+^{(\omega)}$ to $P_-^{(\omega)}$, and EDFA gain G.

C. Receiver Requirements

As discussed in Section V, the anticipated requirement for receiver sensitivity at 10 Gb/s is -20 to -26 dBm. Because of the high quantum efficiency at 775 nm, a Si or GaAs metal-semiconductor-metal (MSM) photodetector is well suited to this application. For such a receiver, the electronic thermal noise will dominate. If we assume a Gaussian-type response $(\eta \approx 2)$ with a 10-GHz bandwidth and 70% quantum efficiency, then to achieve a Q-factor of 6 (10^{-9} BER), (4) implies that the average amplifier noise must be ~7 pA/Hz$^{1/2}$. This level of performance can be realized with current Si and GaAs technology; consequently, it is feasible to design an 775-nm optical receiver that can achieve the required sensitivity at the 10-Gb/s data rate.

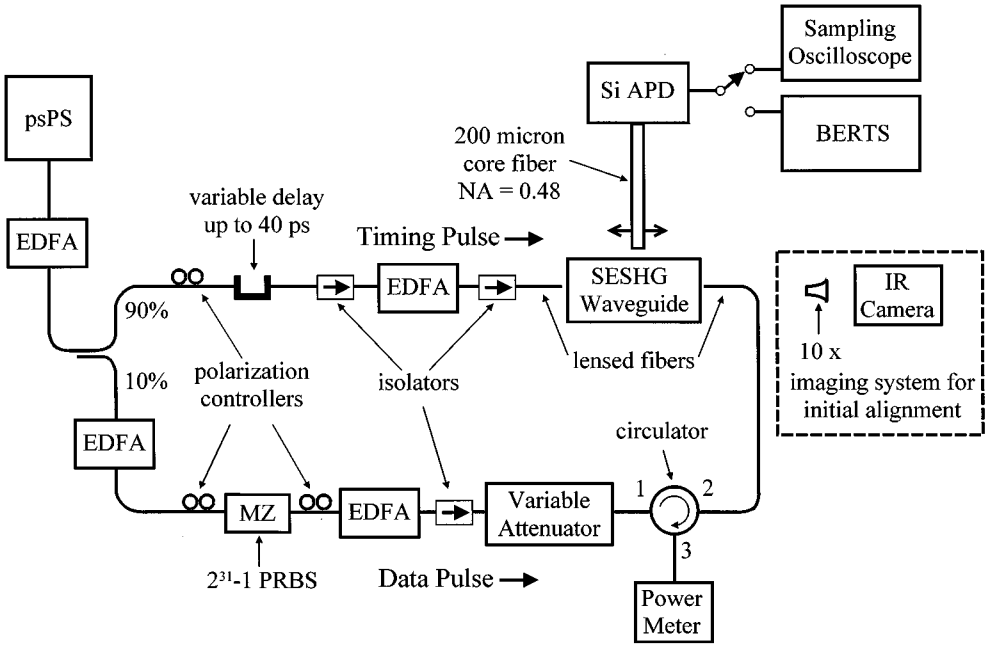

Fig. 10. Experimental setup for the BER measurements. psPS: picosecond-pulse source. EDFA: erbium-doped fiber amplifier. MZ: Mach Zehnder electro-optic modulator. PRBS: pseudo-random bit stream. APD: avalanche photodetector. BERTS: BER test set.

D. Receiver Design

While the technology necessary for a high-sensitivity 10-Gb/s receiver at 775 nm is feasible, such components are not commercially available. For this reason, testing has been performed at 1 and 2.5 Gb/s using a 1-GHz silicon avalanche photodetector (APD) with a multiplication gain of 100, followed by an amplifier that provides an additional gain of 100. The lack of sufficient bandwidth in this APD results in intersymbol interference, which causes closure of the eye by 20% at 2.5 Gb/s; however, the sensitivity of the receiver at 775 nm for a 10^{-9} BER is estimated to be -30 dBm.

In addition to the current Si-APD receiver, a GaAs-based receiver is being designed with a custom MSM and transimpedance amplifier. The MSM has 70% quantum efficiency and at least 10-GHz bandwidth, while the amplifier is expected to have a bandwidth of 8 GHz and an average noise density of 5 pA/Hz$^{1/2}$. As predicted by (4), at 775 nm and 10 Gb/s, this receiver will have a sensitivity of approximately -23 dBm for a 10^{-9} BER.

VII. Demultiplexer Subsystem Testing

We have performed single-channel BER measurements at 1 Gb/s and 2.5 Gb/s using a true colliding-pulse geometry (Fig. 10). The second harmonic is generated in a [211]-oriented waveguide that incorporates a vertical resonant cavity with a 77% top-DBR reflectance. This second-harmonic signal is detected with the 775-nm Si-APD receiver discussed in Section VI. For these experiments, the picosecond-pulse source described in Section II is configured to produce ~ 2 ps pulses near 1548 nm with energies on the order of 1 pJ. These are amplified using an EDFA with a saturated output power of 25 mW. Each pulse is then split with a 90/10 fiber coupler to create a timing pulse and a data pulse. The timing and data pulses travel through equal-length fiber paths and are coupled into the SESHG waveguide from opposite ends. The timing-pulse path contains a free-space variable-delay-line for fine control of the interaction location within the SESHG waveguide, as well as an EDFA that provides an average power of $\sim$32 mW at the entrance facet of the waveguide. The data-pulse path contains a lithium niobate modulator, a variable attenuator, a circulator with a power meter to monitor waveguide coupling, and two EDFAs to provide up to 50 mW of average power at the opposite entrance facet of the waveguide. Autocorrelation measurements show that some distortion of both the timing and data pulses occurs in the EDFAs. Fiber-optic polarization controllers are used to maximize the transmission through the modulator and to set the timing- and data-pulse polarizations to TE at the waveguide facets. Efficient coupling of both the timing-bit stream and the data-bit stream is accomplished by use of lensed fibers. Insertion loss from one lensed fiber through the waveguide to the other lensed fiber is approximately 8 dB. Second-harmonic radiation is collected with a cleaved 200-μm core fiber and coupled to the Si APD module. The variable attenuator allows an assessment of the power dependence of the BER, which is determined using a $(2^{31}-1)$-bit pseudeorandom pattern. Eye diagrams are generated by measuring the APD signal with a 40-GHz sampling oscilloscope.

Error-free performance has been obtained at 1 Gb/s, with a BER below 10^{-12} for estimated counter-propagating pulse energies inside the waveguide of 15 pJ and 45 pJ. The results at 2.5 Gb/s are limited by the power available from the EDFAs, but a BER of 3×10^{-8} was achieved with estimated pulse energies of 6 pJ and 19 pJ inside the waveguide. Importantly, no error floor is observed, suggesting that a 10^{-12} BER is achievable by increasing the 6-pJ pulse energy to 16 pJ. The detected second-harmonic energy with 6-pJ and 19-pJ pulses was 0.8 fJ per pulse at 2.5 Gb/s, resulting in an average power of 1 μW.

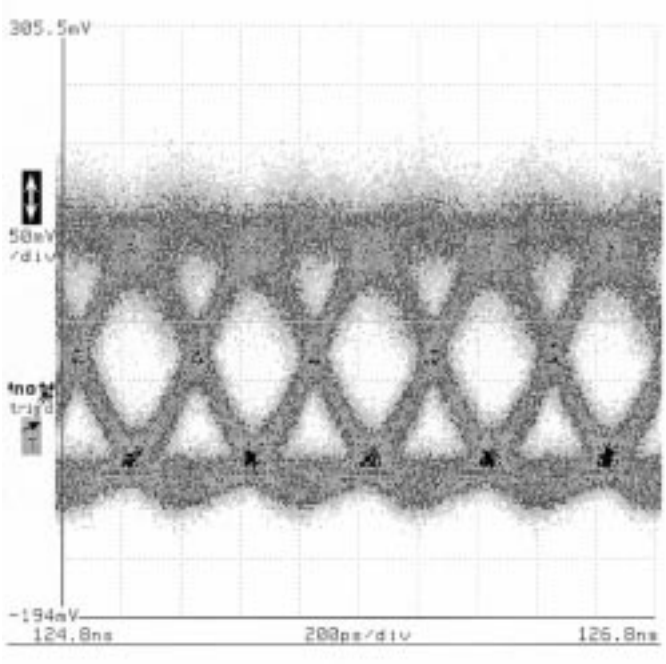

Fig. 11. 2.5-Gb/s eye diagram for a $(2^{31}-1)$-bit pseudorandom pattern.

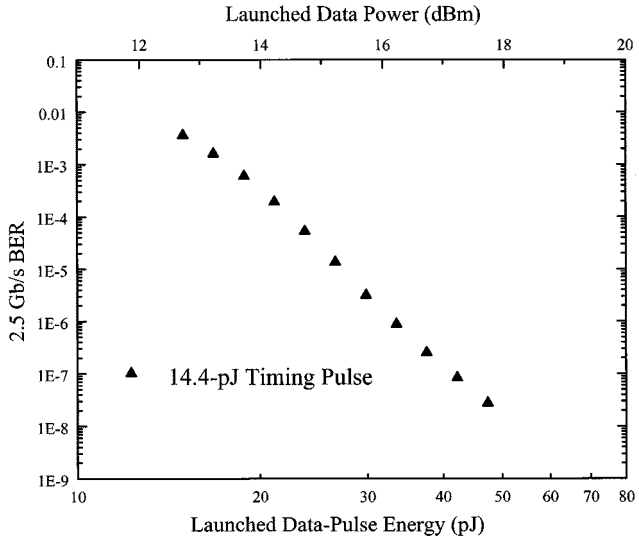

Fig. 12. 2.5-Gb/s BER measurement with a $(2^{31}-1)$-bit pseudorandom pattern.

These energies correspond to a nonlinear cross section of 6.4×10^{-7} W^{-1}, which is a factor of three lower than that measured using an unamplified, nondistorted pulse in the rear-facet reflection configuration. This discrepancy is likely due to uncertainty in the actual power propagating in the waveguide and sub-optimal collection of the SH caused by the temporal distortion of the higher-power pulses. The eye diagram and BER curve for the 2.5-Gb/s experiment are shown in Figs. 11 and 12, respectively. Noise was dominated by optical noise from the EDFAs rather than the electronic noise of the receiver. Analysis of the measured signal-to-noise ratio indicates that improved error rates should be achievable with the same power levels and that performance may be limited by instabilities in the present experimental apparatus.

As can be seen from Fig. 9(a), the optimum top DBR reflectance for 1-ps pulses in this $d = 22\lambda^{SH}/2n$ structure is approximately 98%, and thus the efficiency can be nearly doubled by increasing the top DBR reflectance from its current value of 77%. Furthermore, improvements are possible both in the input coupling (both mode overlap and AR coating) and in the output SH coupling. Waveguide propagation losses, which are presently dominated by scattering due to sidewall roughness, may be reduced by improved processing. Finally, as shown in Fig. 9(b), the enhancement from the cavity can be increased by an additional 40% by decreasing the cavity size.

VIII. Conclusions

We have described experimental and numerical assessments of each of the components necessary to produce a fully populated 160-Gb/s OTDM link. We have demonstrated error-free performance of the central component, the all-optical time-division demultiplexer. The short-pulse source has been completely characterized at 2.5 GHz and initial tests at 5.0 GHz have been completed. The elements of the IOTM have each been experimentally demonstrated. The design considerations for a fiber channel capable of 1-ps pulse transport have been discussed.

The SESHG S/P converter offers key advantages in its simplicity, compact nature, and ability to recover all multiplexed channels with a single operation. The enhanced efficiency of the vertical microcavity combined with the elimination of deleterious absorption effects has allowed the first-ever BER measurements on an SESHG demultiplexer. Non-optimized AlGaAs resonant-cavity-enhanced devices have already shown an improvement of 25 in efficiency over preliminary GaAs-based devices, and the further improvement expected from final optimization of the resonant cavity will allow operation with power levels compatible with 160-Gb/s OTDM fiber-optic systems.

Acknowledgment

The authors would like to thank TriQuint Semiconductor for fabrication of the GaAs transimpedance amplifiers, Nortel Networks for the DFB lasers, and Corning for the planar glass waveguides and the various fibers used in this effort.

References

[1] M. Nakazawa, E. Yoshida, T. Yamamoto, E. Yamada, and A. Sahara, "TDM single channel 640 Gbit/s transmission experiment over 60 km using 400 fs pulse train and walk-off free, dispersion-flattened nonlinear optical loop mirror," *Electron. Lett.*, vol. 34, pp. 907–908, Apr. 1998.

[2] B Mikkelsen, G. Raybon, R.-J. Essiambre, J. E. Johnson, K. Dreyer, and L. F. Nelson, "Unrepeatered transmission over 150 km of nonzero-dispersion fiber at 100 Gbit/s with semiconductor based pulse source, demultiplexer and clock recovery," *Electron. Lett.*, vol. 35, pp. 1866–1868, Oct. 1999.

[3] R. A. Barry, V. W. S. Chan, K. L. Hall, E. S. Kintzer, J. D. Moores, K. A. Rauschenbach, E. A. Swanson, L. E. Adams, C. R. Doerr, S. G. Finn, H. A. Haus, E. P. Ippen, W. S. Wong, and M. Hanner, "All-optical network consortium-ultrafast TDM networks," *IEEE J. Select. Areas Commun.*, vol. 14, pp. 999–1013, Sept. 1995.

[4] H. Anis, G. Berkey, G. Bordogna, M. Cavallari, B. Charbonnier, A. Evans, I. Hardcastle, M. Jones, G. Pettitt, B. Shaw, V. Srikant, and J. Wakefield, "Continuous dispersion managed fiber for very high speed soliton systems," in *Proc. 25th ECOC'99*, vol. 1, Nice, France, Sept. 26–30, 1999, pp. 230–231.

[5] S. Kawanishi, H. Takara, K. Uchiyama, I. Shake, and K. Mori, "3 Tb/s (160 Gb/s × 19 ch) OTDM/WDM transmission experiment," in *Proc. OFC'99*, San Diego, CA, Feb. 21–26, 1999, pp. PD1/1–3.

[6] K. Uchiyama, S. Kawanishi, and M. Saruwatari, "100 Gb/s multiple-channel output all-optical OTDM demultiplexing using multichannel four-wave mixing in a semiconductor optical amplifier," *IEEE Photon. Technol. Lett.*, vol. 10, pp. 890–892, 1998.

[7] U. Keller, K. D. Li, M. Rodwell, and D. M. Bloom, "Noise characterization of femtosecond fiber Raman soliton analyzers," *IEEE J. Quantum Electron.*, vol. 25, pp. 280–288, Mar. 1989.

[8] A. Takada and M. Saruwatari, "100 Gbit/s optical signal generation by time-division multiplication of modulated and compressed pulses from gain-switched distributed feedback (DFB) laser diode," *Electron. Lett.*, vol. 24, pp. 1406–1408, Nov. 1988.

[9] K. Iwatsuki, K. Suzuki, and S. Nishi, "Generation of transform limited gain-switched DFB-LD pulses <6 ps with linear fiber compression and spectral window," *Electron. Lett.*, vol. 27, no. 21, pp. 1981–1982, Oct. 1991.

[10] M. Cavelier, N. Stelmakh, J. M. Xie, L. Chusseau, J.-M. Lourtioz, C. Kazmierski, and N. Bouadma, "Picosecond (<2.5 ps) wavelength-tunable (~ 20 nm) semiconductor laser pulses with repetition rates up to 12 GHz," *Electron. Lett.*, vol. 28, no. 3, pp. 224–226, Jan. 1992.

[11] L. Chusseau and C. Kazmierski, "Optimum linear pulse compression of a gain-switched 1.5 μm DFB laser," *IEEE Photon. Technol. Lett.*, vol. 6, pp. 24–26, Jan. 1994.

[12] K.-I. Suzuki, K. Iwatsuki, S. Nishi, M. Saruwatari, and T. Kitoh, "160 Gb/s sub-picosecond transform-limited pulse signal generation utilizing adiabatic soliton compression and optical time-division multiplexing," *IEEE Photon. Technol. Lett.*, vol. 6, pp. 352–354, Mar. 1994.

[13] M. D. Pelusi, Y. Matsui, and A. Suzuki, "Pedestal suppression from compressed femtosecond pulse using a nonlinear fiber loop mirror," *IEEE J. Quantum Electron.*, vol. 35, pp. 867–874, Jun. 1999.

[14] D. C. Rogers, J. V. Collins, C. W. Ford, J. Lucek, M. Shabeer, G. Sherlock, D. Cotter, K. Smith, C. M. Peed, A. E. Kelly, P. Gunning, D. Nesset, and I. F. Lealman, "Optical pulse pattern generation for self-synchronizing 100 Gbit/s networks," in *Proc. OFC'96*, vol. 2, San Jose, CA, Feb. 25–Mar. 1, 1996, pp. 98–99.

[15] L. Lepetit, G. Cheriaux, and M. Joffre, "Linear techniques of phase measurement by femtosecond spectral interferometry for applications in spectroscopy," *J. Opt. Soc. Amer. B, Opt. Phys.*, vol. 12, pp. 2467–2474, Dec. 1995.

[16] M. K. Chin and W. S. C. Chang, "InGaAs/InAlAs quantum-well electroabsorption waveguide modulators with large-core waveguide structure: Design and characterization," *Appl. Opt.*, vol. 34, pp. 1544–53, 1995.

[17] T. G. Ulmer, M. C. Gross, W. S. Astar, P. W. Juodawlkis, B. R. Washburn, A. J. SpringThorpe, R. P. Kenan, C. M. Verber, and S. E. Ralph, "Ultrafast optical devices for high-speed optical data links," in *Proc. SPIE 44th Annual Meeting: Materials and Devices for Photonic Circuits*, vol. 3803, Denver, CO, July 21–22, 1999, pp. 51–59.

[18] K. Wakita, I. Kotaka, K. Yoshino, S. Kondo, and Y. Noguchi, "Polarization-independent electroabsorption modulators using strain-compensated InGaAs-InAlAs MQW structures," *IEEE Photon. Technol. Lett.*, vol. 7, pp. 1418–20, Dec. 1995.

[19] R. Thurston, E. Kapon, and A. Shahar, "Two-dimensional control of mode size in optical channel waveguides by lateral channel tapering," *Opt. Lett.*, vol. 16, pp. 306–309, Mar. 1991.

[20] G. Vawter, R. Smith, H. Hou, and J. Wendt, "Semiconductor laser with tapered-rib adiabatic following fiber coupler for expanded output diameter," *IEEE Photon. Technol. Lett.*, vol. 9, pp. 425–427, Apr. 1997.

[21] V. Vusirikala, S. S. Saini, R. E. Bartolo, R. Whaley, S. Agarwala, M. Dagenais, F. G. Johnson, and D. Stone, "High butt-coupling efficiency to single-mode fibers using a 1.55 μm InGaAsP laser integrated with a tapered ridge transformer," *IEEE Photon. Technol. Lett.*, vol. 9, pp. 1472–1474, Nov. 1997.

[22] V. Vusirikala, S. S. Saini, R. E. Bartolo, S. Agarwala, R. D. Whaley, F. G. Johnson, D. R. Stone, and M. Dagenais, "1.55-μm InGaAsP-InP laser arrays with integrated-mode expanders fabricated using a single epitaxial growth," *IEEE J. Select. Topics Quantum Electron.*, vol. 3, pp. 1332–1343, Dec. 1997.

[23] G. P. Agrawal, *Nonlinear Fiber Optics*. New York: Academic, 1995.

[24] M. Matsumoto and H. A. Haus, "Stretched-pulse optical fiber communications," *IEEE Photon. Technol. Lett.*, vol. 9, pp. 785–787, June 1997.

[25] T. Yu, E. A. Golovchenko, A. N. Pilipetskii, and C. R. Menyuk, "Dispersion-managed soliton interactions in optical fibers," *Opt. Lett.*, vol. 22, pp. 793–795, June 1997.

[26] B. Mikkelsen, G. Raybon, R.-J. Essiambre, K. Dreyer, Y. Su, L. E. Nelson, J. E. Johnson, G. Shtengel, A. Bond, D. G. Moodie, and A. D. Ellis, "160-Gb/s single-channel transmission over 300 km nonzero-dispersion fiber with semiconductor based transmitter and demultiplexer," in *Proc. 25th ECOC '99*, Nice, France, Sept. 26–30, 1999, PD-28.

[27] C. M. Verber, "Method and apparatus for high data rate fiber optic communication system," U.S. Patent 5 172 258, Dec. 15, 1992.

[28] K. A. Shore, X. Chen, and P. Blood, "Frequency doubling and sum frequency generation in semiconductor optical waveguide devices," *Prog. Quantum Electron.*, vol. 20, no. 3, pp. 181–218, 1996.

[29] R. K. Tan, C. M. Verber, and A. J. SpringThorpe, "Self-timed integrated-optical serial-to-parallel converter for 100 Gbit/s time demultiplexing," *IEEE Photon. Technol. Lett.*, vol. 6, pp. 1228–1230, Oct. 1994.

[30] J. P. Sokoloff, P. R. Prucnal, I. Glesk, and M. Kane, "A terahertz optical asymmetric demultiplexer (TOAD)," *IEEE Photon. Technol. Lett.*, vol. 5, pp. 787–790, July 1993.

[31] D. Zhou, I. Kang, I. Glesk, and P. R. Prucnal, "An analysis of signal-to-noise ratio and design parameters of a terahertz optical asymmetric demultiplexer," *J. Lightwave Technol.*, vol. 17, pp. 298–307, Feb. 1999.

[32] O. Boyraz, J. W. Lou, K. H. Ahn, Y. Liang, T. J. Xia, Y. H. Kao, and M. N. Islam, "Demonstration and performance analysis for the off-ramp portion of an all-optical access node," *J. Lightwave Technol.*, vol. 17, pp. 998–1010, June 1999.

[33] N. S. Patel, K. A. Rauschenbach, and K. L. Hall, "40-Gb/s demultiplexing using an ultrafast nonlinear interferometer (UNI)," *IEEE Photon. Technol. Lett.*, vol. 8, pp. 1695–1697, Dec. 1996.

[34] K. Uchiyama, S. Kawanishi, and M. Saruwatari, "100-Gb/s multiple-channel output all-optical OTDM demultiplexing using multichannel four-wave mixing in a semiconductor optical amplifier," *IEEE Photon. Technol. Lett.*, vol. 10, pp. 890–892, June 1998.

[35] M. L. Dennis, W. K. Burns, T. F. Carruthers, and I. N. Duling III, "Eight-to-one demultiplexing of 100-Gbit/s TDM data using LiNbO3 Sagnac interferometric modulators," in *Proc. OFC'98*, vol. 2, San Jose, CA, Feb. 22–27, 1998, pp. 110–112.

[36] M. L. Dennis, W. K. Burns, T. F. Carruthers, W. I. Kaechele, and I. R. Duling III, "Photonic 100 Gb/s serial-to-parallel converter," in *Proc. OFC'2000*, Baltimore, MD, Mar. 2000, Paper ThV1.

[37] R. Normandin, R. L. Williams, and F. Chatenoud, "Enhanced surface emitting waveguides for visible, monolithic semiconductor laser sources," *Electron. Lett.*, vol. 26, no. 25, pp. 2088–2089, Dec. 1990.

[38] P. A. Ramos and E. Towe, "Second-order nonlinear polarization and harmonic generation in [11*l*]-oriented III–V heterostructures," *Opt. Commun.*, vol. 132, pp. 121–127, Nov. 1996.

[39] D. Vakhshoori, "Analysis of visible surface-emitting second-harmonic generators," *J. Appl. Phys.*, vol. 70, no. 10, pp. 5205–5210, Nov. 1991.

[40] R. Lodenkamper, M. M. Fejer, and J. S. Harris Jr., "Surface emitting second harmonic generation in vertical resonator," *Electron. Lett.*, vol. 27, no. 20, pp. 1882–1884, Sept. 1991.

[41] R. Lodenkamper, M. L. Bortz, M. M. Fejer, K. Bacher, and J. S. Harris Jr., "Surface-emitting second-harmonic generation in a semiconductor vertical resonator," *Opt. Lett.*, vol. 18, no. 21, pp. 1798–1800, Nov. 1993.

[42] Y. J. Ding, J. B. Khurgin, and S. J. Lee, "Cavity-enhanced and quasi-phase-matched optical frequency doublers in surface-emitting geometry," *J. Opt. Soc. Amer. B, Opt. Phys.*, vol. 12, pp. 1586–1594, Sept. 1995.

[43] Y. J. Ding and J. B. Khurgin, "Spatial and temporal effects in second-harmonic generation from mode-locked lasers in surface-emitting geometry," *J. Appl. Phys.*, vol. 82, no. 10, pp. 4732–4739, Nov. 1997.

[44] S. Janz, Y. Beaulieu, A. Fiore, P. Bravetti, V. Berger, E. Rosencher, and J. Nagle, "Surface emitted second-harmonic generation from a quasi-phase matched waveguide in an $Al_xGa_{1-x}As/Al_2O_3$ microcavity," *Opt. Express*, vol. 2, pp. 462–470, June 1998.

[45] R. Normandin and G. I. Stegeman, "Nondegenerate four-wave mixing in integrated optics," *Opt. Lett.*, vol. 4, pp. 58–59, Feb. 1979.

[46] R. Normandin, S. Létourneau, F. Chatenoud, and R. L. Williams, "Monolithic, surface-emitting, semiconductor visible lasers and spectrometers for WDM fiber communication systems," *IEEE J. Quantum Electron.*, vol. 27, pp. 1520–1530, June 1991.

[47] A. Ashkin, G. D. Boyd, and J. M. Dziedzic, "Resonant optical second harmonic generation and mixing," *IEEE J. Quantum Electron.*, vol. QE-2, pp. 109–124, June 1966.

[48] D. I. Babic and S. W. Corzine, "Analytic expressions for the reflection delay, penetration depth, and absorptance of quarter-wave dielectric mirrors," *IEEE J. Quantum Electron.*, vol. 28, pp. 514–524, Feb. 1992.

[49] T. G. Ulmer, R. K. Tan, Z. Zhou, S. E. Ralph, R. P. Kenan, C. M. Verber, and A. J. SpringThorpe, "Two-photon absorption-induced self-phase modulation in GaAs-AlGaAs waveguides for surface-emitted second-harmonic generation," *Opt. Lett.*, vol. 24, no. 11, pp. 756–758, June 1999.

[50] P. J. Winzer and A. Kalmar, "Sensitivity enhancement of optical receivers by impulsive coding," *J. Lightwave Technol.*, vol. 17, pp. 171–177, 1999.
[51] L. Boivin, M. C. Nuss, J. Shah, D. A. B. Miller, and H. A. Haus, "Receiver sensitivity improvement by impulsive coding," *IEEE Photon. Technol. Lett.*, vol. 9, pp. 684–686, 1997.
[52] S. D. Personick, "Receiver design for digital fiber optic communication systems I," *Bell Syst. Tech. J.*, vol. 52, pp. 843–874, 1973.
[53] S. Wang and M. Ingram, "Performance analysis of an optical serial-to-parallel converter with erbium-doped fiber amplifier," *J. Lightwave Technol.*, vol. 14, pp. 2736–2748, 1996.

Todd G. Ulmer was born in Pennsylvania in 1970. He received the B.S. degree in physics (magna cum laude) from Furman University, Greenville, SC, in 1993, and the B.E.E. degree with highest honors and the M.S. degree in electrical engineering from the Georgia Institute of Technology (Georgia Tech), Atlanta, in 1994 and 1996, respectively. He is currently pursuing the Ph.D. in electrical engineering at Georgia Tech.

He has been a Member of the Ultrafast Optical Communications Group of Georgia Tech since 1993. His research interests include high-capacity fiber-optic communications and nonlinear optics.

Mr. Ulmer is a member of Phi Beta Kappa, the IEEE Lasers and Electro-Optics Society, and the Optical Society of America (OSA). He is a Recipient of the Schlumberger Foundation Fellowship and a 2000 SAIC Student Paper Award.

Michael C. Gross was born in Atlanta, GA, in 1972. He received the B.S. degree in electrical engineering from Rice University, Houston, TX, in 1995 and the M.S. degree in electrical engineering from the Georgia Institute of Technology (Georgia Tech), Atlanta, in 1996. He is currently pursuing the Ph.D. degree in electrical engineering at Georgia Tech, working in the Ultrafast Optical Communications Group.

His research interests include gain-switched laser diodes, passively mode-locked fiber lasers, and pulse compression.

Mr. Gross is a member of the IEEE Lasers and Electro-Optics Society, the Optical Society of America (OSA), and Eta Kappa Nu. He has received the Shackleford Research Fellowship, the Metz Scholarship, the Allen Scholarship, and the National Merit Scholarship.

Ketan M. Patel received the B.S.E. and M.S.E. degrees in electrical engineering from the University of Michigan, Ann Arbor, in 1993 and 1995, respectively. He is currently pursuing the Ph.D. degree in optical communications at the Georgia Institute of Technology, Atlanta.

In 1995, he joined the Microwave Electronics Group of Texas Instruments, Dallas, which later became part of TriQuint Semiconductor. His research interests include fiber-optic communications, integrated optics, and integrated microwave electronics.

Julaine T. Simmons was born in Miami, FL, in 1976. She received the B.S. degree in electrical engineering from the Florida Institute of Technology, Melbourne, in 1998 and the M.S. degree in electrical engineering from the Georgia Institute of Technology (Georgia Tech), Atlanta, in 2000.

While at Georgia Tech, she was a Georgia Tech Presidential Fellow. While a Member of the Bell Labs Summer Internship Program, she developed high-powered, double-clad fiber lasers and amplifiers, and she studied the impairments of four-wave mixing in OC-192 DWDM systems. Currently, she is a Member of Technical Staff in the Advanced Optical Networking Group of Lucent Technologies, Holmdel, NJ.

Mrs. Simmons is a member of Tau Beta Pi, the IEEE Lasers and Electro-Optics Society, and the Optical Society of America (OSA).

Paul W. Juodawlkis (S'86–M'86) was born in Detroit, MI, in 1964. He received the B.S. degree (*summa cum laude*) in electrical engineering from Michigan Technological University, Houghton, in 1986, the M.S. degree in electrical engineering, specializing in solid-state circuit design, from Purdue University, Lafayette, IN, in 1988, and the Ph.D. degree in electrical engineering from the Georgia Institute of Technology (Georgia Tech), Atlanta, in 1999. His thesis research focused on the optoelectronic properties and device applications of low-temperature-grown semiconductor quantum-well materials.

While at Georgia Tech, he worked in the Ultrafast Optical Communications Laboratory. From 1988 to 1993, he was a Technical Staff Member at MIT Lincoln Laboratory, Lexington, MA, working as a Hardware Systems Engineer on a multi-sensor airborne testbed program. After completing his Ph.D. degree, he rejoined Lincoln Laboratory as a Member of the Electro-Optic Materials and Devices group and is presently involved in the development of analog-to-digital converters utilizing optical sampling techniques. His research interests include laser noise characteristics, ultrashort pulse generation and applications, optical nonlinearities, and optoelectronic interfaces.

Dr. Juodawlkis is a member of the IEEE Lasers and Electro-Optics Society, the Optical Society of America (OSA), and AAAS. He is a recipient of the Georgia Tech President's Fellowship, the Schlumberger Foundation Fellowship, and the SPIE Scholarship in Optical Engineering.

Brian R. Washburn received the B.S. degree from the University of Wisconsin, Parkside, in 1994. He is currently pursuing the Ph.D. degree in physics at the Georgia Institute of Technology, Atlanta.

In 1995, he held a research position at Argonne National Laboratory working on high-temperature superconductors. His research interests include ultrafast semiconductor spectroscopy, nonlinear fiber optics, and the characterization of ultrashort optical pulses.

Mr. Washburn is a member of the American Physical Society and the IEEE Lasers and Electro-Optics Society.

William S. Astar received the B.S. degrees in electrical and mechanical engineering from the University of South Florida in 1987 and 1994, respectively, and the M.S. degree in electrical engineering from the University of Central Florida in 1990.

He held a technical position at Pall Aeropower Co., as part of a team designing and testing pressure swing adsorption filtration systems for military applications. His interests include OTDM and WDM telecommunication systems, Raman and erbium-doped fiber amplifiers, soliton communication systems, pulse compression, and the design, analysis, and packaging of semiconductor and silica waveguide devices.

Mr. Astar is a member of SPIE, the Optical Society of America (OSA), the American Society of Mechanical Engineers, and Pi Tau Sigma.

Anthony J. SpringThorpe, photograph and biography not available at the time of publication.

Richard P. Kenan (M'82–SM'89) received the B.S. degree in physics from the Georgia Institute of Technology (Georgia Tech), Atlanta, in 1955 and the Ph.D. degree in physics (solid state) from the Ohio State University, Columbus, in 1962.

He was with Battelle Memorial Institute, Columbus, for 24 years, where his research concentrated on magnetism, the band structure of insulating solids, optics, and integrated optics. In 1986, he joined the faculty of the School of Electrical and Computer Engineering at Georgia Tech. He is the author of over 90 technical articles and presentations, and holds ten U.S. patents.

Dr. Kenan is a Fellow of the Optical Society of America (OSA).

Carl M. Verber (M'74–SM'86) received the B.S. degree from Yale University, New Haven, CT, the M.S. degree from the University of Rochester, Rochester, NY, and the Ph.D. degree from the University of Colorado, Boulder, all in physics.

He has worked at the Columbus Laboratory of Battelle Memorial Institute, where he was responsible for providing technical guidance for the optics activities of the Electronics Department and where he established the Optical Sciences Group. He holds the Byers Eminent Scholar in Microelectronics chair in the School of Electrical and Computer Engineering at the Georgia Institute of Technology, Atlanta. His research interests include nuclear magnetic resonance, optical properties of materials, and the development of optical communication systems. He is the author of over 60 technical papers on optics and integrated optics and holds 13 U.S. patents.

Dr. Verber is a Fellow of the Optical Society of America (OSA).

Stephen E. Ralph (S'86–M'87) received the B.E.E. degree in electrical engineering from the Georgia Institute of Technology, Atlanta, in 1980 and the Ph.D. degree in electrical engineering from Cornell University, Ithaca, NY, in 1988. His research focused on the optical detection of highly nonequilibrium transport in heterojunction devices.

In 1988, he began a Post-Doctoral position at AT&T Bell Laboratories. In 1990, he joined the IBM T. J. Watson Research Center. In 1992, he joined the faculty of the Physics Department, Emory University. In May of 1998, he became an Associate Professor of Electrical and Computer Engineering at the Georgia Institute of Technology, where his work currently focuses on the development of ultrafast optical devices for telecommunications.

Dr. Ralph is a member of the American Physical Society, the IEEE Lasers and Electro-Optics Society, and the Optical Society of America (OSA).